Intracellular pH dynamics respond to microenvironment stiffening and mediate vasculogenic mimicry through β-catenin

Leah M. Lund[1,2], Angelina N. Marchi[1,2], Laura Alderfer[3,5], Eva Hall[3], Jacob Hammer[1,2], Keelan J. Trull[1,2], Donny Hanjaya-Putra[2,3,4] and Katharine A. White[1,2]

[1]Department of Chemistry and Biochemistry, University of Notre Dame
251 Nieuwland Science Hall
Notre Dame, IN 46556 USA

[2]Harper Cancer Research Institute, University of Notre Dame
1234 N. Notre Dame Avenue
South Bend, IN 46617 USA

[3]Bioengineering Graduate Program, Aerospace and Mechanical Engineering, University of Notre Dame
153 Multidisciplinary Engineering Research Building
Notre Dame, IN 46556 USA

[4]Chemical and Biomolecular Engineering, University of Notre Dame
250 Nieuwland Hall
Notre Dame, IN 46556 USA

[5]Current: Vivodyne
Suite 775 601 Walnut Street
Philadelphia PA 19106 USA

Abstract

Dysregulated intracellular pH (pHi) dynamics and an altered tumor microenvironment have emerged as drivers of cancer cell phenotypes. However, the molecular integration between the physical properties of the microenvironment and dynamic intracellular signaling responses remains unclear. Here, we use two metastatic cell models, one breast and one lung, to assess pHi response to varying extracellular matrix (ECM)

1

34   stiffness. To experimentally model ECM stiffening, we use two tunable-stiffness

35   hydrogel systems: Matrigel and hyaluronic acid (HA) gels, which mimic the increased

36   protein secretion and crosslinking associated with ECM stiffening. We find that single-

37   cell pHi decreases with increased ECM stiffness in both hydrogel systems and both

38   metastatic cell types. We also observed that stiff ECM promotes vasculogenic mimicry

39   (VM), a phenotype associated with metastasis and resistance. Importantly, we show

40   that decreased pHi is both a necessary and sufficient mediator of VM, as raising pHi on

41   stiff ECM reduces VM phenotypes and lowering pHi on soft ECM drives VM. We

42   characterize β-catenin as a pH-dependent molecular mediator of pH-dependent VM,

43   where stiffness-driven changes in β-catenin abundance can be overridden by increased

44   pHi. We uncover a dynamic relationship between matrix stiffness and pHi, thus

45   suggesting pHi dynamics can override mechanosensitive cell responses to the

46   extracellular microenvironment.

47

48   **Introduction**

49   The extracellular matrix (ECM) is a protein-rich structure that becomes

50   dysregulated in cancer, driving cancer cell adaptation and promotion of cancer cell

51   phenotypes[1]. This increasingly rigid and dense tumor ECM has been shown to promote

52   cancer cell invasion and vasculogenic mimicry, an adaptive cancer phenotype [2,3]. In

53   addition to the dysregulated extracellular environment, cancer cells also experience

54   dysregulated pH dynamics[4], with increased intracellular pH (pHi) (>7.4) and decreased

55   extracellular pH (pHe) (<7.2) compared to normal epithelial cells (pHi 7.0-7.3; pHe 7.4)[5].

56   This reversal of the pH gradient is an early event in cellular transformation[6] and has

2

57   been directly linked to adaptive changes in cancer cell signaling, metabolism,

58   proliferation, and evasion of apoptosis[5].

59   Increased ECM stiffness promotes various cancer cell phenotypes including

60   increased hypoxia[7], vasculogenic mimicry[8], cell durotaxis[9], and selection for tumor

61   initiating cell (TIC) or cancer stem-cell phenotypes[4,10–13]. Importantly, many equivalent

62   or similar processes are also linked to dysregulated pHi dynamics including hypoxia[11],

63   cell invasion[4], and maintenance of a stem-like phenotype in adult and embryonic stem

64   cell models[14]. However, the molecular mechanisms that integrate the physical

65   properties of the microenvironment with intracellular cancer cell signaling response are

66   largely unknown.

67   While prior work has shown pHi dynamics can directly regulate normal

68   mechanosensitive behaviors including focal adhesion remodeling[15] and epithelial cell-

69   cell contacts[16,17], there are significant gaps in knowledge of the molecular crosstalk

70   between ECM stiffening and pHi dynamics in cancer cells. One limitation is technical: it

71   is challenging to develop mechanically tunable model systems that mimic physiological

72   ECM dysregulation with suitable mechanical control. Previous studies have used

73   synthetic ECM models, including Matrigel/Geltrex[18] and Hyaluronan[19] based systems.

74   However, these studies have lacked the ability to decouple the contributions of ECM

75   protein abundance and ECM crosslinking density as independent drivers of

76   mechanosensitive cell responses.

77   Another limiting factor in characterizing molecular links between ECM stiffness

78   and pHi is that most mechanistic studies of how pHi dynamics regulate cell behaviors

79   are performed under non-physiological culture conditions and lack single-cell resolution.

3

80   These limitations apply to most studies of pHi dynamics in biology, but are compounded

81   when exploring effects of physical forces on cellular pHi dynamics and in the context of

82   phenotypically heterogeneous cancer cells.

83   Here, we pair synthetic tunable-stiffness ECM models with live-cell pHi

84   measurements and non-invasive pHi manipulation to elucidate how pHi dynamics

85   respond to ECM stiffening. We further explore a mechanistic role of pHi in regulating a

86   cancer-associated mechanosensitive phenotype called vasculogenic mimicry (VM). We

87   use two unique synthetic matrix models to mimic ECM stiffening through increasing

88   protein abundance (Matrigel/Geltrex) and crosslinking density (hyaluronic acid gels),

89   and measure single-cell pHi in metastatic breast and lung cancer cells. We show that

90   pHi decreases with increased stiffness using both matrix models. We also show that

91   cells plated on stiff ECM acquire distinct VM phenotypes that can be modulated by

92   dynamically altering pHi. Importantly, raising pHi in cells plated on stiff matrix reduces

93   VM phenotypes while lowering pHi in cells plated on soft matrix induces acquisition of a

94   stiffness-independent VM phenotype. We also investigate the pH dependence of two

95   molecular regulators of VM that have been previously shown to be regulated by ECM

96   stiffness (β-catenin and FOXC2). We show that β-catenin is a pH-dependent mediator

97   of VM phenotype while FOXC2 activity is pHi insensitive in this system. This suggests

98   β-catenin as a novel necessary regulator of pH-dependent vasculogenic mimicry.

99   Overall, our work reveals a previously unidentified link between mechanosensing and

100   pHi dynamics in cancer and further suggests low pHi as a necessary and sufficient

101   mediator of VM, a phenotype associated with aggressive cancers.

102

103   **Results**

104   **Stiffening extracellular matrix lowers pHi in metastatic human lung carcinoma**

105   Increased tumor microenvironment (TME) stiffness can be caused by increased

106   ECM protein deposition and increased crosslinking[20] (Figure 1A). To investigate the

107   central hypothesis of how a stiffening extracellular environment alters pHi, we used two

108   tunable-stiffness hydrogel models to control ECM stiffness with high specificity and

109   using two unique modes of mechanical modulation. To mimic the effects of ECM

110   stiffness changes resulting from altered ECM protein crosslinking, we used a

111   hyaluronic-acid (HA) gel system where variable crosslinking density tunes ECM

112   stiffness independent of protein concentration and composition[21,22]. HA is a non-sulfated

113   linear polysaccharide of (1-β-4)d-glucuronic acid and (1-β-3)N-acetyl-d-glucosamine,

114   and is a ubiquitous component of the ECM[19]. HA is particularly abundant in the

115   extracellular environment of the lung and brain[19], and increased HA secretion is

116   associated with cancers[19] as well as fibrotic diseases of the liver and lung[23].

117   Recent work has shown that HA can be functionalized to contain thiol-reactive

118   cross-linkable regions, with increased crosslinking adding rigidity to the ECM allowing

119   tunable stiffness[24]. Our HA gel tunable-stiffness model consists of a uniform mixture of

120   gelatin and thiol-modified hyaluronan across stiffnesses, while stiffness is controlled by

121   modulating amounts (%) of thiol-reactive PEGDA crosslinker (see methods for details).

122   The HA gel model consists of four levels of crosslinking agent mimicking ECM stiffness

123   changes induced by increased protein crosslinking and has a previously reported

124   tunable stiffness range from ~100-1500 Pa[25] (Figure 1B). This system allows us to

125   modulate matrix stiffness by adjusting the extent of ECM protein crosslinking while

126 maintaining a consistent concentration of matrix components (hyaluronan and gelatin)

127 across all stiffness conditions. This ability to model ECM stiffness independent of matrix

128 concentration is a unique feature which provides advantage over model systems which

129 use natural hydrogels in decoupling individual drivers of ECM stiffening.

130
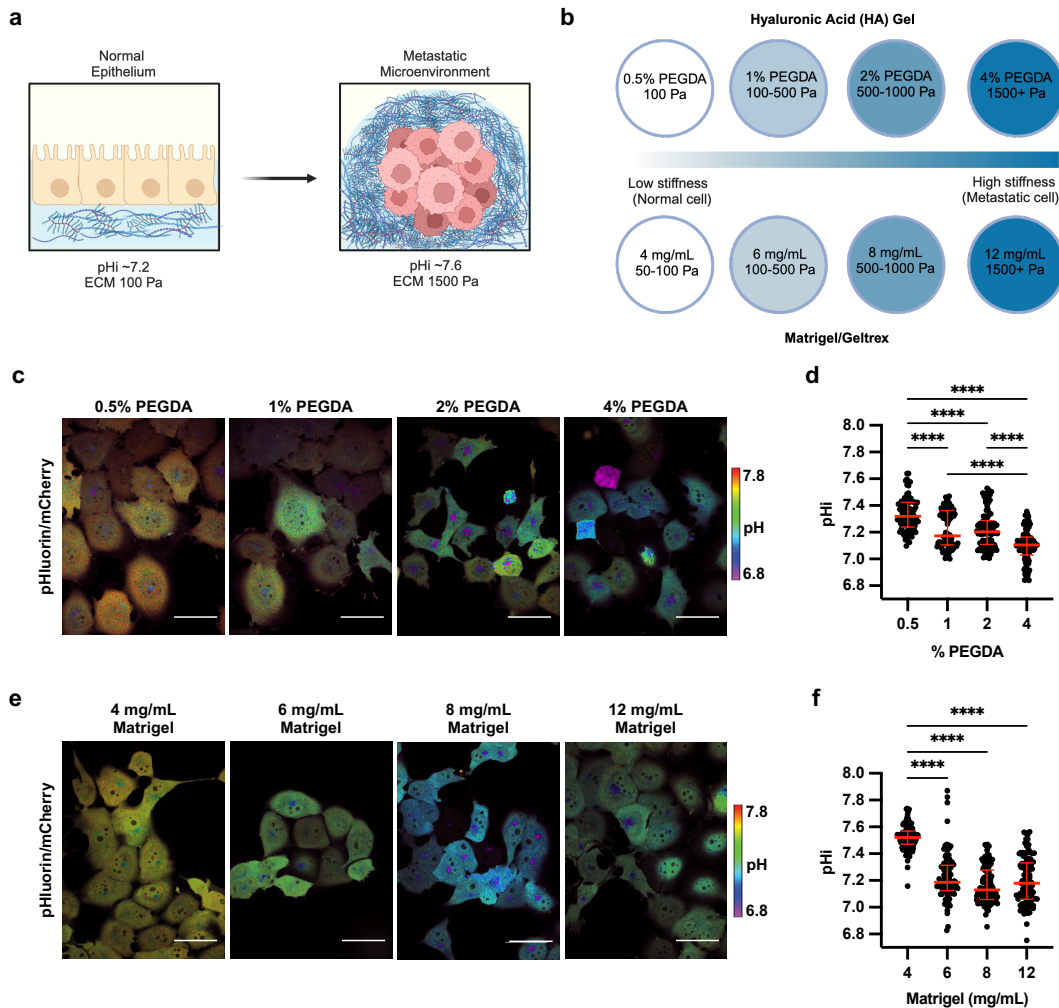
Figure 1: Stiffening extracellular matrix lowers pHi in metastatic human lung carcinoma (H1299). a) Schematic of increased pHi and ECM stiffening (via increased protein secretion and increased protein crosslinking) associated with tumorigenesis. **b)** Schematic of synthetic ECM models with tunable-stiffness (~50 Pa-1,500 Pa). The Matrigel (or Geltrex) model mimics increased ECM protein secretion while hyaluronic acid (HA) gel system mimics increased ECM protein crosslinking. **c)** Representative images of H1299 cells stably expressing mCherry-pHluorin pH biosensor plated on varying HA gel stiffnesses. Images show ratiometric display of pHluorin/mCherry fluorescence. Scale bars: 50 μm. **d)** Quantification of single-cell pHi data collected as

140   shown in (c). (n=3 biological replicates; n=91 0.5% PEGDA, n=90 1% PEGDA, n=102
141   2% PEGDA, n=89 4% PEGDA. Red lines show medians ± IQR). **e)** Representative
142   images of H1299 cells stably expressing mCherry-pHluorin pH biosensor plated on
143   varying Matrigel stiffnesses. Images show ratiometric display of pHluorin/mCherry
144   fluorescence. Scale bars: 50 µm. **f)** Quantification of single-cell pHi data collected as
145   shown in (e). (n=3 biological replicates; n=93 4mg/mL, n=92 6mg/mL, n=102 8mg/mL,
146   n=97 12mg/mL. Red lines show medians ± IQR). For (d) and (f), significance was
147   determined by a Kruskal-Wallis test (****P<0.0001).
148

149   To mimic the effects of stiffness changes due to increased ECM protein

150   secretion, we used a Matrigel- or Geltrex-based tunable-stiffness gel system. Matrigel

151   and Geltrex are naturally-derived matrices that mimic the tumor microenvironment of

152   stromal-rich tissues, such as breast, lung, and prostate[26]. The Matrigel and Geltrex

153   commercial matrix mixtures are rich in laminin and collagen; EMC proteins that directly

154   promote integrin signaling[27]. Varying the concentration of Matrigel and Geltrex

155   effectively titrates ECM protein concentrations[28], mimicking the increased secretion of

156   ECM proteins associated with stiffening tumor microenvironment[29]. We used tunable-

157   stiffness Matrigel/Geltrex models that consist of four Matrigel/Geltrex concentrations (4

158   mg/mL-12 mg/mL) with stiffness ranges of ~50-1,500 Pa[30–32] (Figure 1B). For these

159   stiffness determinations, the manufacturer reports an elastic modulus (G′) that can be

160   converted to Young's modulus (matrix stiffness) using the following equation $E= 2G'(1 +$

161    $v)$. Prior work has indicated that hydrogels can be assumed to be incompressible, such

162   that their Poisson's ratio (v) approaches 0.5[33], simplifying the equation to $E=3G'$

163   Importantly, in the Matrigel/Geltrex tunable-stiffness gel systems, as the ECM protein

164   concentrations increase, so does the available ligand concentration for integrin-

165   mediated interactions. This gel model allows us to assess effects of ECM stiffening on

166   pHi when intracellular integrin signaling is also titrating.

7

167   With the two tunable-stiffness hydrogel systems established, we next selected

168   cancer cell lines that originated from tissues with a relatively soft ECM, such as lung

169   and breast, where tumorigenic ECM stiffening has been associated with both increased

170   metastasis and invasion[26]. We have previously established and characterized single-cell

171   pHi heterogeneity in a clonal metastatic lung cancer cell line (H1299) and a clonal

172   breast cancer cell line (MDA-MB-231), all plated and imaged on glass[34]. We have

173   engineered these cell lines to stably express a genetically-encoded ratiometric pH

174   biosensor mCherry-pHluorin (mCh-pHl)[34]. This biosensor is a fusion of the fluorescent

175   protein pHluorin (pKa 7.1) that is pH-sensitive in the physiological range, and the

176   fluorescent protein mCherry, that is pH-insensitive in the physiological range[35]. For

177   accurate pHi measurements in single cells, ratiometric imaging of pHluorin and mCherry

178   fluorescence can be performed followed by single-cell standardization using isotonic

179   buffers with a known pHi containing the protonophore Nigericin to equilibrate

180   intracellular and extracellular (buffer) pH[36]. Single-cell standard curves are then

181   generated, enabling back-calculation of pHi from pHluorin and mCherry fluorescence

182   intensity ratios (Supplemental Figure 1, see methods for details). This biosensor has

183   successfully been used in prior studies to measure single-cell spatiotemporal pHi

184   dynamics in clonal cancer and normal epithelial cell populations without affecting cell

185   morphology or behavior[15,34,35].

186   To determine effects of altered ECM stiffness on pHi, we cultured H1299 cells

187   expressing the mCh-pHl biosensor on matrix-coated imaging dishes for 48 hours. This

188   incubation allowed for cells to adhere and respond to the varied stiffness of each matrix

189   system. In cells plated on HA gels, single-cell pHi decreased with increasing stiffness

190　(Figure 1D). Cells plated on the stiffest matrix (4% PEGDA) had a significantly

191　decreased pHi (Figure 1D; 7.10±0.07; median±interquartile range (IQR)) compared to

192　cells on the softest matrix (0.5% PEGDA) (Figure 1D; 7.32±0.10; median±IQR). We also

193　observed that intermediate ECM stiffnesses (1% PEGDA and 2% PEGDA) produced

194　intermediate effects on pHi, with a stepwise trend of decreasing pHi with increasing

195　stiffness (Figure 1F; 2% PEGDA 7.20±0.10; 1% PEGDA 7.17±0.19; medians±IQR). The

196　overall decrease in pHi of ~0.2 pH units between soft and stiff ECM is within the range

197　of physiological pHi dynamics that have been shown to regulate normal cell behaviors

198　including cell cycle progression[34], differentiation[13,37], and migration[38]. This result shows

199　that stiffening of the ECM through changes in protein crosslinking drives significant

200　decreases in single-cell pHi of clonal metastatic lung cancer cells. These data suggest

201　that progressive changes in ECM stiffness within the physiological range of normal to

202　metastatic mechanical stiffness environments can alter pHi in metastatic cancer cells,

203　suggesting a potential role for pHi in mechanosensitive cancer cell signaling and

204　behaviors.

205　　　　We next determined whether the stiff ECM decreased pHi using the Matrigel

206　tunable-stiffness models, where ECM protein concentration is the predominant driver of

207　altered stiffness. In cells plated on varied Matrigel stiffnesses, single-cell pHi decreased

208　with increasing stiffness (Figure 1E). Cells plated on the stiffest matrix (12 mg/mL) had

209　a significantly decreased pHi (7.18±0.15; median±IQR) compared to the softest matrix

210　(4 mg/mL; 7.52±0.49; median±IQR) (Figure 1F). The decrease in pHi of ~0.35 units

211　between stiffest (~1,500 Pa) and softest (~50 Pa) ECM in this system is also consistent

212　with the pHi changes we measured between stiffest and softest HA gel models.

213   However, in the Matrigel tunable-stiffness model system, the pHi measured on

214   intermediate stiffnesses (6 mg/mL Matrigel, 7.19±0.13; 8 mg/mL Matrigel, 7.13±0.14;

215   medians±IQR) was not significantly different from the pHi of cells plated on a stiff matrix

216   (Figure 1F). This result shows that ECM stiffening decreases pHi in metastatic cells via

217   both increased ECM protein abundance and crosslinking, showing mechanism

218   independent ECM stiffness driven pHi dynamics in metastatic cells.

219   We next confirmed that ECM stiffness leads to decreased pHi using metastatic

220   breast epithelial cell model (MDA-MB-231) as another metastatic cell model derived

221   from a stromal-rich environment. The pHi of MDA-MB-231 cells was decreased by ~0.2

222   units in cells plated on a stiff matrix compared to soft matrix in both the Matrigel (soft

223   7.40±0.14; stiff 7.20±0.13; median±IQR) and HA gel (soft 7.43±0.14; stiff 7.28±0.10;

224   median±IQR) models (Supplemental Figure 1). Taken together, these data show that

225   increases in ECM stiffness mediated by either increased crosslinking (HA gel model) or

226   by increased ECM protein secretion (Matrigel model) both decrease pHi at the single-

227   cell level. Our data also show that the stiffness-dependent decreases in pHi are not

228   tissue specific as both breast and lung metastatic models exhibited a 0.2-0.35 decrease

229   in pHi on stiff compared to soft matrices. In summary, these data show that there is an

230   inverse relationship between ECM stiffening and pHi in these metastatic cancer cell

231   models, and further suggests a role for pHi in regulating pH-sensitive molecular

232   pathways to drive or reinforce stiffness-associated phenotypes.

233

234

Stiffness dependent vasculogenic mimicry is reduced in high pHi conditions in metastatic lung carcinoma

When performing the single-cell pHi measurements on tunable-stiffness ECM models, we also observed a distinct change in overall cancer cell morphology that correlated with increased ECM stiffness. Metastatic cancer cells plated on soft matrix grew in flat lawns of large rounded (H1299) or spindle-shaped cells (MDA-MB-231), forming a near-confluent sheet. However, on stiff matrix, the metastatic cancer cells grew in compact clusters of irregularly shaped cells, frequently exhibited 3D growth phenotypes, and formed connected bridges of significantly elongated spindle shaped cells between 3D "nodes" (Supplemental Figure 3). This change in cell morphology we observed on stiff matrices has been previously described as a vasculogenic mimicry (VM) phenotype. VM is an aggressive cancer phenotype observed both *in vivo* and *in vitro*, where tumor cells organize into vessel-like structures, allowing nutrients and oxygen access independent of traditional angiogenesis[39]. Previous studies have shown increased ECM stiffness can drive VM[40] phenotypes and have also characterized 2D VM phenotypes as a pronounced growth pattern where cells form distinct networks of tightly packed cells with surrounding open space devoid of cell growth[41].

Our data showing single-cell pHi decreases in H1299 cells on stiff ECM led to the hypothesis that low pHi is a necessary mediator of VM and that raising pHi in H1299 cells plated on stiff matrix would reduce the VM phenotype (Figure 2A). To directly test this hypothesis, we established protocols to experimentally raise pHi in H1299 cells plated on stiff ECM. Prior work showed that 50 mM Sodium Bicarbonate supplemented into the media for 24 hours was sufficient to raise pHi in H1299 cells plated on glass[34].

11

258   We imaged single-cell pHi in H1299 cells plated on soft ECM, stiff ECM, and stiff ECM

259   with bicarbonate supplementation (Figure 2B). We found that bicarbonate significantly

260   increased pHi of cells plated on stiff ECM compared to untreated cells on stiff matrix

261   (stiff 7.27±0.08; stiff + Bicarbonate 7.43±0.08; median±IQR) (Figure 2C). While the

262   absolute pHi achieved with bicarbonate treatment on stiff HA gel matrix was lower than

263   the matched pHi of control cells plated on soft ECM (Figure 2C), the bicarbonate

264   treatment increased the pHi of cells plated on the stiffest ECM by approximately 0.2 pH

265   units (Figure 2C), which is similar to the magnitude of pHi changes we observed

266   between soft and stiff ECM across the various cell lines and gel systems.

267   We next tested the effects of increased pHi on the stiffness-dependent

268   vasculogenic mimicry phenotype. We found that H1299 cells acquired a vasculogenic

269   mimicry phenotype on stiff matrix, and this VM phenotype was abrogated when pHi was

270   increased on stiff matrix (Figure 2D). Cells plated on stiff matrix with bicarbonate-

271   induced increases in pHi grew in a 2D cobblestone-like morphology similar to the

272   morphology of cells grown on the soft ECM (Figure 2D, additional representative

273   images in Supplemental Figure 4). To confirm that the observed pH-dependent change

274   in cell morphology was not due to pH-dependent or stiffness-dependent differences in

275   cell proliferation, we assayed proliferation rates in H1299 cells plated on soft and stiff

276   ECM with and without increased pHi. Importantly, we did not observe any significant

277   differences in proliferation rates across our experimental conditions (Figure 2E). Our

278   data showing loss of VM networks when pHi is increased in cells plated on stiff ECM

279   demonstrate that low pHi is necessary to maintain VM phenotypes on stiff ECM.

280   Furthermore, these data show that high pHi can override stiffness-dependent

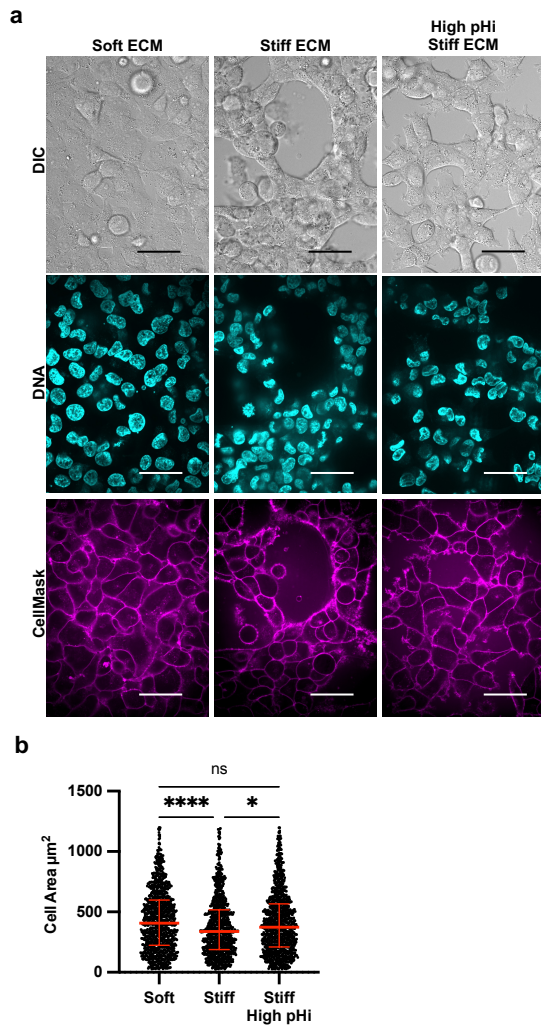281   vasculogenic mimicry in a metastatic cancer model.

282
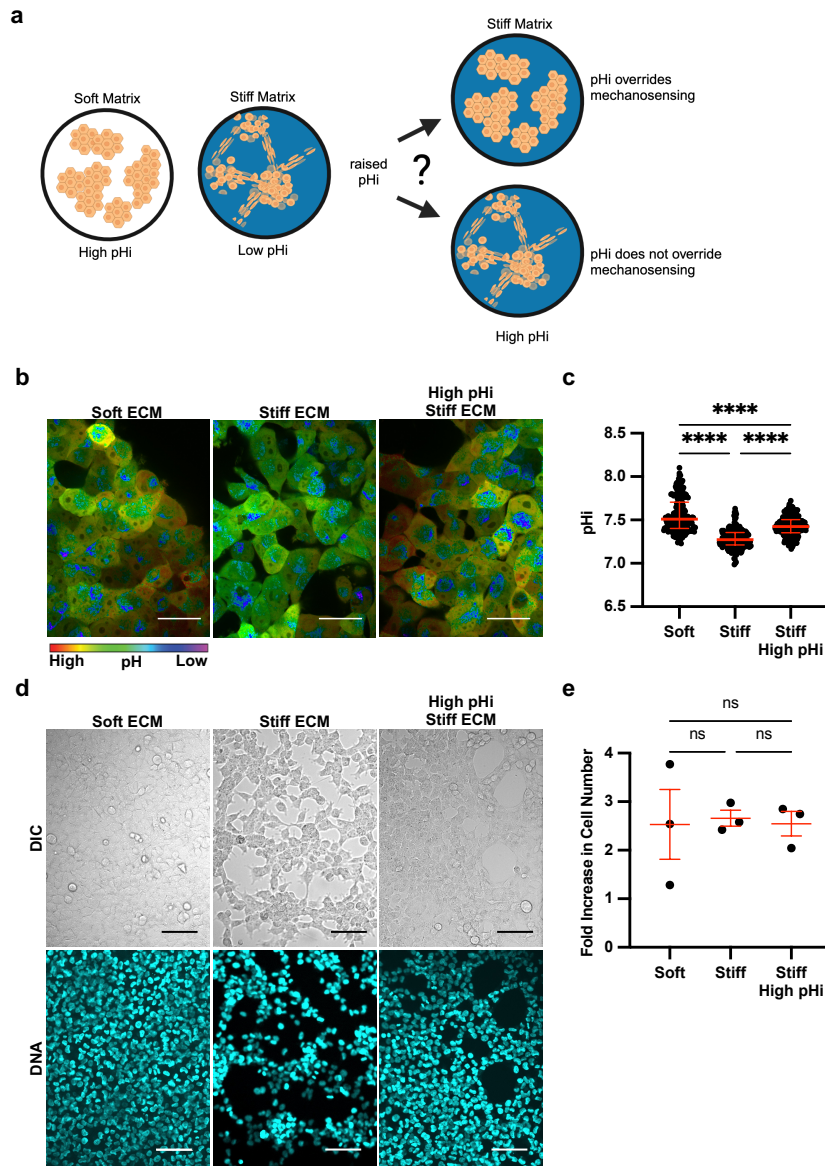
Figure 2: Stiffness-dependent vasculogenic mimicry is reduced when pHi is increased on stiff ECM. a) Schematic of vasculogenic mimicry (VM) in 2D on stiffening matrix. **b)** Representative images of H1299 cells stably expressing mCherry-pHluorin pH biosensor plated on soft (0.5% PEGDA) and stiff (4% PEGDA) HA gels and stiff (4% PEGDA) with raised pHi. Images show ratiometric display of pHluorin/mCherry fluorescence ratios. Scale bars: 50 μm. **c)** Quantification of single-cell pHi data collected as shown in (b) (n=3 biological replicates; n=201 soft, n=237 stiff, n=239 stiff high pHi. Red lines show medians ± IQR). **d)** Representative images of H1299 cells plated on soft

291   (0.5% PEGDA) and stiff (4% PEGDA) HA gels. Images show differential interference

292   contrast (DIC) and Hoechst stain (DNA, cyan). Scale bars: 100 μm. **e)** Quantification of

293   cell proliferation across manipulation conditions. (n=3 biological replicates, n=9 per

294   condition. Red lines show means ± SEM).

295

296   To quantify the observed stiffness- and pHi-dependent changes in cell

297   morphology, we used a cell membrane marker and quantitative image analysis (see

298   methods for details) pipeline to assess cell area (Figure 3A). Notably, single-cell area of

299   H1299 cells was significantly lower in cells plated on stiff ECM compared to soft ECM

300   (Figure 3B; stiff 338.6 $\mu m^2 \pm 189$; soft 406.5 $\mu m^2 \pm 224.6$; median±IQR). This result

301   demonstrates that cell area is a robust quantitative morphology indicator that decreases

302   with acquisition of VM phenotype on stiff ECM. This allows us to quantitatively

303   distinguish cell morphologies corresponding to low VM and high VM conditions.

304   Importantly, we found that cell area significantly increased (Figure 3C; 374.3

305   $\mu m^2 \pm 210.6$; median±IQR) when pHi was raised in H1299 cells plated on stiff ECM

306   compared to control H1299 on stiff ECM (Figure 3B). This indicates that increased pHi

307   attenuates the observed stiffness-dependent VM phenotype. The loss of VM networks

308   and increased cell area when pHi is raised on stiff ECM demonstrates that low pHi is

309   required for cells to acquire VM on stiff matrices. Together, our findings confirm

310   previous literature characterizing vasculogenic mimicry as an ECM stiffness-mediated

311   phenotype and further identifies decreased pHi as a previously unrecognized necessary

312   regulator of VM.

313

Figure 3: Vasculogenic mimicry phenotype decreases cell area on stiff ECM, which is rescued by increasing pHi in metastatic lung carcinoma. a) Representative images of H1299 cells plated on soft (0.5% PEGDA) and stiff (4% PEGDA) HA gels and stiff (4% PEGDA) with raised pHi. Images show differential interference contrast (DIC), Hoechst 33342 (DNA, cyan) and CellMask Deep Red membrane stain (Cy5, magenta). Scale bars: 50 μm. **b)** Quantification of single-cell area collected as shown in (a) (n=3 biological replicates, n=1061 soft, n=954 stiff, n=1078 stiff high pHi. Red lines show medians ± IQR).

314
315
316
317
318
319
320
321
322

323

324

β-catenin abundance is stiffness-dependent, pHi-dependent, and necessary for stiffness-dependent vasculogenic mimicry

We next investigated potential molecular drivers of pH-dependent regulation of VM. In epithelial cells, VM is regulated by several characterized mechanisms, including the activity and abundance of β-catenin[42,43]. β-catenin is a multifunctional protein involved in cell-cell adhesion and transcription. Previous work has shown that both whole cell abundance and transcriptional activity of β-catenin directly regulate VM[42]. A recent study using malignant melanoma cells showed that knockdown of β-catenin or silencing of its co-transcriptional activator transcription factor 4 (TCF4) disables VM phenotypes[42]. Additionally, previous work has shown that increased nuclear localization of β-catenin correlates with VM formation in colon cancer cells[43] and is associated with a stiffening ECM in liver cancer cells[44]. Importantly, ECM stiffening has also been shown to increase whole-cell β-catenin abundance in some cell lines, including human mesenchymal stem cells[45,46]. While previous studies have demonstrated the role of β-catenin in regulating VM, these studies have not characterized the cellular cues by which a stiff ECM increases β-catenin abundance or nuclear localization.

Our prior work has shown that high pHi reduces stability of β-catenin in normal canine kidney (MDCK) epithelial cells, leading to loss of β-catenin from adherens junctions[47]. More recently, we have shown that low pHi stabilizes β-catenin and increases the transcriptional activity in MDCK epithelial cells[17]. Further, this study showed that β-catenin abundance and nuclear localization were decreased when pHi was raised, suggesting pHi acts as a rheostat to modulate β-catenin abundance and adhesion and signaling functions[17]. However, our prior work did not assess pH-

16

348   dependent β-catenin stability in non-epithelial models and did not characterize the

349   functional consequences of pH-dependent β-catenin stability on cell behaviors. Thus,

350   we next tested the hypothesis that stiffness-associated pHi dynamics modulate VM

351   through regulation of β-catenin abundance in metastatic cancer cell lines.

352   To determine the effect of ECM stiffening on β-catenin abundance in metastatic

353   cancer cells, we performed immunofluorescent staining of β-catenin in H1299 cells

354   plated on soft ECM and stiff ECM both with and without pHi manipulation (Figure 4A). In

355   agreement with prior work[46], we found that whole-cell abundance of β-catenin was

356   significantly increased in cells plated on stiff ECM compared to cells plated on soft ECM

357   (Figure 4B). Furthermore, we found that when we raised pHi in cells plated on stiff ECM,

358   β-catenin abundance was significantly reduced compared to control cells plated on stiff

359   ECM (Figure 4B). We also determined the effects of ECM stiffening and pHi modulation

360   on nuclear localization of β-catenin. We quantified the intensity of β-catenin within single

361   cell nuclei and found that β-catenin nuclear abundance was significantly increased on

362   stiff compared to soft ECM (Figure 4C). When pHi was raised in cells plated on a stiff

363   matrix, β-catenin nuclear intensity was significantly decreased compared to cells plated

364   on a stiff matrix in the absence of pHi manipulation (Figure 4C). These data show that

365   increased β-catenin abundance is correlated with low pHi in a human clonal metastatic

366   cancer cell line and confirm our hypothesis that β-catenin is a pH-dependent regulator

367   of stiffness-dependent vasculogenic mimicry. These data show that high pHi can

368   override mechanosensing by decreasing β-catenin abundance, suggesting that low pHi

369   functions as a necessary mediator of VM in cancer cells via stabilization of β-catenin

370   abundance.
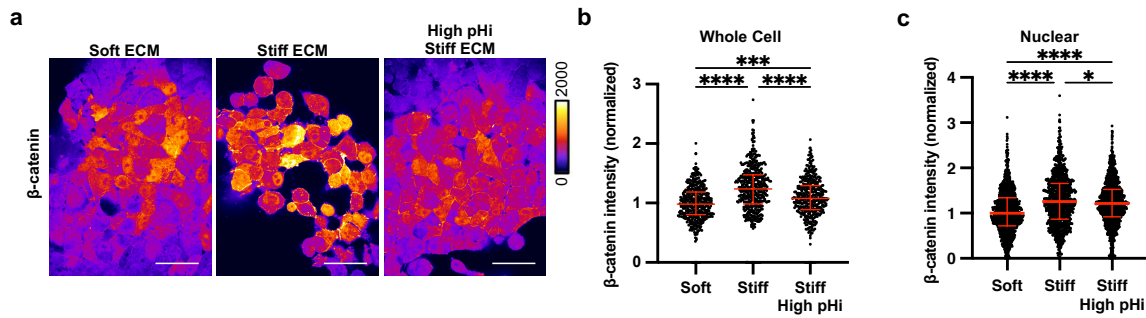
Figure 4: Increased pHi reduced β-catenin abundance and nuclear localization in stiff matrix conditions. a) Representative images of H1299 cells plated on soft (0.5% PEGDA), stiff (4% PEGDA) and stiff with raised pHi (4% PEGDA) HA gels fixed and stained for β-catenin. β-catenin is pseudocolored according to scale. Scale bars: 50 μm. **b)** Quantification of whole cell β-catenin intensity collected as shown in (a). (n=3 biological replicates, n=452 soft, n=486 stiff, n=415 stiff high pHi. Red lines show medians ± IQR). **c)** Quantification of nuclear β-catenin intensity collected as described in (a). (n=3 biological replicates, n=1043 soft, n=975 stiff, n=1157 stiff high. Red lines show medians ± IQR). For (b) and (c), significance was determined by a Kruskal-Wallis test (*$P<0.05$; **$P<0.01$; ***$P<0.001$; ****$P<0.0001$).

FOXC2 activity is stiffness-dependent, pHi-independent, and not sufficient for vasculogenic mimicry

It is possible that other molecular regulators of VM also exhibit pHi-sensitive activity and contribute to the abrogation of stiffness-associated VM phenotypes at high pHi. Increased expression and activity of the transcription factor FOXC2 has previously been shown to promote VM in ovarian cancer[41] and breast cancer cells[48] by upregulating expression of VM associated genes. However, while FOXC2 has been shown to be required for VM[48], and sufficient to drive endothelial cell vascularization[49], it is unclear whether FOXC2 abundance or activity is a sufficient driver of VM phenotypes. Furthermore, existing literature is conflicting as to whether FOXC2 and β-catenin are independent drivers of VM. For example, significant prior data suggests that β-catenin functions upstream of FOXC2 in VM, with β-catenin being shown to directly control

18

395   expression of FOX transcription factors[49]. However, other data suggests that FOXC2

396   can directly induce Wnt signaling[50,51] and rescues acquisition of vasculogenic mimicry

397   when β-catenin levels are reduced[49]. Our data showing that β-catenin is a pH-

398   dependent molecular mediator of VM allows us to explore both independence and

399   crosstalk between FOXC2 and β-catenin in regulating stiffness- and pH-dependent VM

400   phenotypes.

401   We first measured FOXC2 abundance and activity in our model of metastatic

402   lung cancer cells that form VM phenotypes. We performed immunofluorescent staining

403   of FOXC2 in H1299 cells plated on soft ECM and stiff ECM and found that whole-cell

404   abundance of FOXC2 was the same in H1299 cells plated on soft vs. stiff matrix

405   (Supplemental Figure 5A,B). This suggests that whole cell abundance of FOXC2 is not

406   regulated by ECM stiffness in these cells. We next measured FOXC2 transcriptional

407   activity in single cells. We performed single-cell analysis of FOXC2 transcriptional

408   activity using a highly specific FOXC2-TAG-Puro reporter plasmid with FOXC2 specific

409   tandem repeats flanking a core DNA binding element upstream of GFP (LipExoGen,

410   see methods). Increased FOXC2 DNA binding and transcription drives increased GFP

411   fluorescence (Supplemental Figure 5C). We performed these single-cell transcriptional

412   assays in H1299 cells plated on soft ECM and on stiff ECM with and without increased

413   pHi. We found that FOXC2 activity was significantly increased in cells plated on stiff

414   ECM compared to cells plated on soft ECM, suggesting that ECM stiffening is sufficient

415   to increase FOXC2 transcriptional activity (Supplemental Figure 3D, E). However, we

416   found that FOXC2 transcriptional activity was not altered when pHi was increased on a

417   stiff matrix (Supplemental Figure 3D,E). This result demonstrates that high pHi does not

19

418 decrease FOXC2 activity in cells on a stiff matrix, suggesting that pHi dynamics do not

419 override stiffness-driven increases in FOXC2 activity. Furthermore, our data show that

420 high FOXC2 transcriptional activation is not a sufficient driver of VM, as high pHi

421 abrogates VM phenotypes without altering FOXC2 transcriptional activity. Our data also

422 suggest that β-catenin loss at high pHi overrides VM independently of FOXC2 activity,

423 reducing VM phenotypes even while FOXC2 transcription remains high.

424   The prior results suggest that increased pHi can override stiffness-associated VM

425 phenotypes. We next hypothesized that low pHi is a sufficient mediator of VM and that

426 lowering pHi in H1299 cells plated on soft matrix would induce stiffness-independent

427 acquisition of VM phenotypes. To directly test this hypothesis, we used an H1299 cell

428 line that is deficient in the sodium proton exchanger (H1299-NHE1 K.O., see methods).

429 This H1299-NHE1 K.O. cell line has significantly decreased pHi (7.35±0.04) compared

430 to parental H1299 (7.60±0.03) (Figure 5A). Importantly, incubating the H1299-NHE1

431 K.O. cell line with bicarbonate raised pHi to the pHi of parental H1299 (7.62±0.04)

432 Figure 5A). We performed an acid load recovery assay to confirm that the H1299-NHE1

433 K.O. cell line had no measurable NHE1 activity (Figure S6A). Using this experimental

434 system, we tested the effects of decreased pHi on modulating VM phenotypes. We

435 found that the H1299-NHE1 K.O. cells acquired a VM phenotype on soft matrix,

436 suggesting low pHi is indeed a sufficient driver of VM in the absence of stiff ECM

437 mechanical cues (Figure 5B). Importantly, the stiffness-independent VM phenotype

438 observed in H1299-NHE1 K.O. cells on soft ECM was abrogated when pHi was

439 increased in these cells on the soft matrix (Figure 5B). We again used cell area to

440 quantify extent of VM phenotype and found that when pHi is lowered (H1299-NHE1

441   K.O.) in cells plated on soft ECM, single-cell area is significantly decreased compared to

442   when the same cells plated on soft ECM but were manipulated to have a high pHi

443   (Figure 5C). Our findings demonstrate that decreased pHi is sufficient to drive VM

444   phenotype in the absence of stiffening ECM mechanical cues. Again, we confirm that

445   increasing pHi is sufficient to override VM phenotypes, even when VM is aberrantly

446   generated on soft ECM.
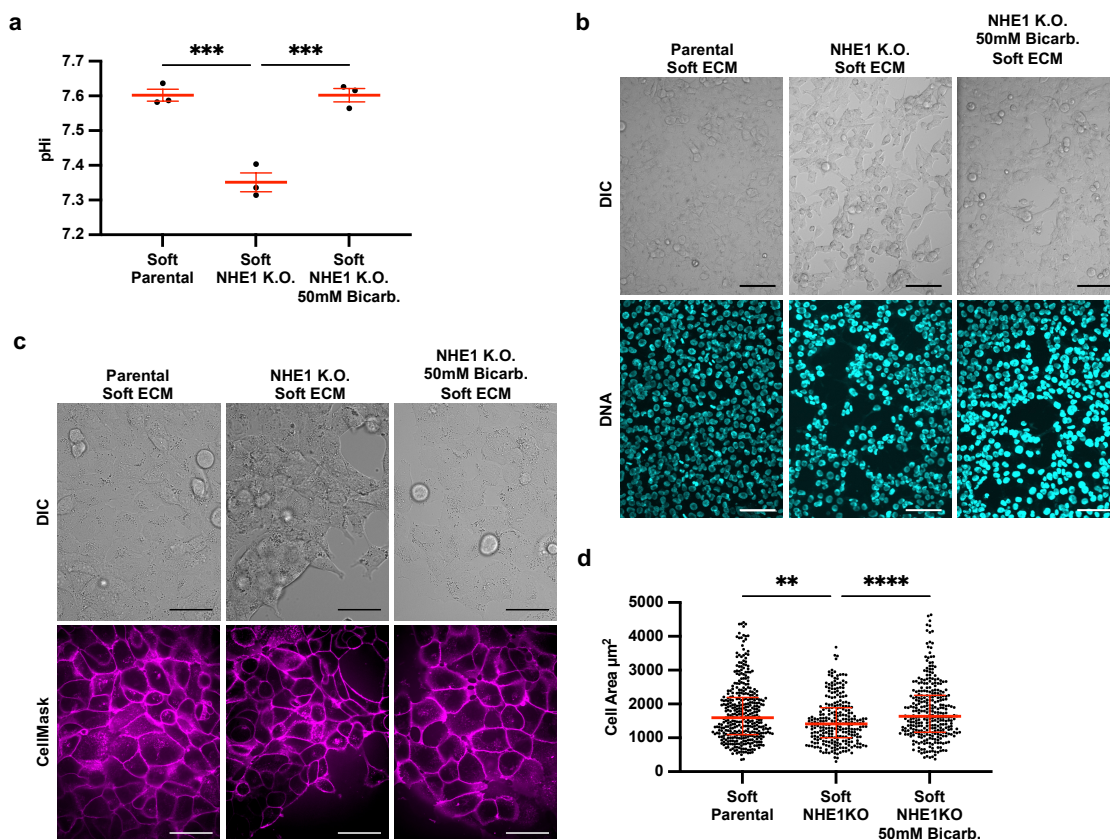
447

448   **Figure 5: Low pHi is sufficient to induce vasculogenic mimicry on a soft ECM. a)**
449   Quantification of pHi data from parental H1299 cells and H1299 cells where NHE1
450   knockout via CRISPR (H1299-NHE1 K.O.). with and without treatment with sodium
451   bicarbonate (Bicarb.) (see methods) (n=3 biological replicates. n=9 parental, n=18
452   NHE1 K.O., n=18 NHE1 K.O. Bicarb. Red lines show means ± SEM). **b)** Representative
453   images of H1299 cells plated on soft HA gels (0.5% PEGDA) with and without lowered
454   pHi (H1299-NHE1 K.O.) and with or without increased pHi (H1299-NHE1 K.O. Bicarb.).
455   Images show differential interference contrast (DIC) and Hoechst 33342 (DNA, cyan).
456   Scale bars: 100 μm. **c)** Representative images of H1299 cells plated on soft HA gels

457 (0.5% PEGDA) with and without lowered pHi (H1299-NHE1 K.O.) and with or without

458 increased pHi (H1299-NHE1 K.O. Bicarb.). Images show differential interference

459 contrast (DIC) and CellMask Deep Red membrane stain (Cy5, magenta). Scale bars: 50

460 μm. **d)** Quantification of single-cell area collected as shown in (a) (n=3 biological

461 replicates, n=383 parental, n=267 NHE1 K.O., n=315 NHE1 K.O. Bicarb. Red lines

462 show medians ± IQR).

463

464 **Discussion**

465   Our work identifies pHi dynamics as a previously unrecognized regulator of

466 stiffness-dependent VM in metastatic cancer cell models. We combined physiologically

467 relevant tunable-stiffness hydrogel systems with single-cell pHi imaging and quantitative

468 microscopy approaches to reveal novel molecular integration of the extracellular

469 mechanical environment and pHi. We show that increasing ECM stiffness, driven by

470 either increased protein concentration or crosslinking, lowers the single-cell pHi of both

471 lung and breast metastatic cell lines. Most previously described tumorigenic behaviors

472 such as hyperplasia[52], metastatic progression[34,53], and drug resistance[53] are

473 associated with increased pHi. However, recent work suggests a potential role for

474 comparatively low cancer cell pHi in regulating hypoxia response[54] and modulating

475 tumor initiating cell (or tumor stem cell) phenotypes[14]. Adding to these recent data, our

476 new findings show that low pHi in cancer cells is both a necessary and sufficient driver

477 of VM. When we raise pHi in cells plated on stiff ECM, we attenuate VM phenotypes,

478 overriding mechanosensitive regulation of VM. More surprisingly, low pHi was sufficient

479 to drive formation of VM phenotypes on soft ECM (in the absence of mechanical

480 stiffening).

481   Our work characterizing pH-dependent molecular drivers of VM identified β-

482 catenin as a pH-sensitive regulator of vasculogenic mimicry. We also show that another

483 VM regulator, FOXC2 has stiffness-dependent, but pHi-*independent*, activity. Our

22

484   molecular characterization of VM regulators using tunable-stiffness hydrogels in

485   combination with pHi manipulation approaches also resolved conflicting data in the

486   literature on the interdependence of β-catenin and FOXC2 in VM regulation.

487   Importantly, our data suggest that β-catenin is a necessary regulator of stiffness-

488   dependent VM and that FOXC2 transcriptional activation is not sufficient to drive VM in

489   the absence of stabilized β-catenin.

490   Our data reveal that pHi is a master regulator of VM and can override

491   mechanosensitive phenotypes in 2D, revealing an improved understanding of molecular

492   mechanisms driving cancer cell adaptive behaviors in the context of a stiffening ECM. In

493   this work, we limit our characterization to 2D ECM models and a few metastatic cell

494   models and focus on just one tumorigenic mechanosensitive phenotype (VM). This

495   approach enables us to combine single-cell pHi measurements and pHi manipulation

496   with tunable-stiffness hydrogel systems that enable differentiation of contributions of

497   stiffness and pHi in these complex cell morphology phenotypes. Our findings provide

498   the groundwork for future experiments investigating pHi-dependent mechanosensitive

499   behaviors in more complex 3D tumor spheroid models or even co-culture models with

500   cancer associated fibroblasts or immune cells. Prior work has already independently

501   shown that more complex 3D environments produce increased vasculogenic mimicry

502   and phenotypic heterogeneity[55] and pronounced pHi gradients[56]. Our current findings

503   motivate expanding these studies to more complex mechanical and cellular

504   environments to explore mechanistic roles for pHi dynamics in regulating other

505   mechanosensitive tumorigenic behaviors such as durotaxis, invasion, and phenotypic

506   plasticity (or dedifferentiation).

507

508

Methods

Cell Culture

H1299 (parental ATCC CRL-5803) or H1299-NHE1 K.O. (CRISPRed cell line was a gift

from Dr. Diane Barber at the University of California, San Francisco) were grown in

RPMI 1640 (Corning, 10-040-CV) supplemented with 10% Fetal Bovine Serum (FBS,

Peak Serum, PS-FB2).

MDA-MB-231 (ATCC HTB-26) cells were grown in DMEM (Corning, MT10013CVV)

supplemented with 10% FBS. All cells were maintained at 5% CO_2 and 37°C in a

humidified incubator. To increase pHi, cells were cultured under normal conditions for

24 hours before being treated for 24 hours with culture media supplemented to a final

concentration of 50mM Sodium Bicarbonate (Sigma-Aldrich; S6297-250G).

Transient Expression and Stable Cell Line Generation

H1299 and MDA-MB-231 mCherry-pHluorin expressing cells were generated as

previously described[34]. FOXC2-TAG-Puro (LipExoGen Biotech, SKU:LTV-0061)

positive H1299 cells were generated using lentiviral article transduction. Briefly, H1299

cells were plated at 50% confluency in a 6 well tissue culture treated plate. After 24

hours, media was replaced with fresh media containing 10ug/mL of polybrene and

50uL/well of FOXC2-TAG-Puro lentiviral particles. Cells were incubated for 72 hours

prior to selection with 0.8 mg/mL blasticidin (Thermo Fisher Scientific, BP264725). After

4 weeks of selection, GFP positive cells were sorted on a BD FACS ARIA III cell sorter

24

530   using 488nm excitation with 515nm-545nm emission filter. These cells were collected

531   into 1mL 1XPBS using high purity sort settings. Cells were then centrifuged and plated

532   in complete RPMI media with 0.8 mg/mL blasticidin.

533

534   *Preparation of tunable-stiffness hydrogels*

535   *Matrigel or Geltrex gel systems*

536   Matrigel (Corning 356231, Lot 9035003) or Geltrex (Gibco, A14132-02, add LOT)

537   coated plates were made in 35 mm diameter, 4-well (9.5 mm/well) glass bottom dishes

538   (Matsunami, D141400). Stock Matrigel or Geltrex (12 or 16 mg/mL respectively) were

539   diluted in cold complete media to concentrations of 4 mg/mL, 6 mg/mL, and 8 mg/mL

540   which cover a range of stiffness from 50 Pa to ~1000 Pa[30–32]. Each well was coated with

541   2.6 μL matrix per mm of well surface area (25 μL/well for 9.5 mm 4-well plate). Matrix

542   was allowed to solidify at 37°C for 20 minutes prior to cell plating. Cells were plated at

543   5,000 cells per well in 100 μL solution volume.

544

545   *HA gel system*

546   HyStem-C (Advanced BioMatrix GS313) gels are composed of thiol-modified hyaluronic

547   acid (Glycosil, GS222F), thiol-modified gelatin (Gelin-S, GS231F), polyethylene glycol

548   diacrylate (PEGDA, Extralink, GS3007F), and degassed, deionized water (DG

549   Water)[22,30]. Basement matrix solution was made of 1:1 Glycosil and Gelin-S and varying

550   final PEGDA percentages (0.5, 1, 2, and 4%) were prepared in degassed, deionized

551   water. The basement matrix solution and respective percentage PEGDA were mixed in

552   a 4:1 parts ratio immediately before plating. Each well was coated with 1.4 μL matrix per

25

553   mm of well surface area (13.5 µL/well). Cells were plated on the pre-prepared synthetic

554   ECM plates 48 hours prior to imaging at 5,000 (single-cell pHi measurements) or 75,000

555   (VM imaging/staining) cells/well in 100 µL solution volume. HA gels were pre-prepared a

556   maximum of 3 days prior to plating of cells, and stored with Dulbecco's phosphate

557   buffered saline (DPBS) (Quality Biological, 114-057-101) in each well to maintain

558   hydration at 4°C.

559

560   *Microscope System*

561   Confocal images were collected on a Nikon Ti-2 spinning disk confocal with a 10x

562   (PLAN APO NA0.45) air objective, 40x (CFI PLAN FLUOR NA1.3) oil immersion

563   objective, and 60x (PLAN APO NA1.4) oil immersion objective. The microscope is

564   equipped with a stage-top incubator (Tokai Hit), a Yokogawa spinning disk confocal

565   head (CSU-X1), four laser lines (405 nm (100 mW), 488 nm (100 mW), 561 nm (100

566   mW), 640 nm (75 mW)), a Ti2-S-SE motorized stage, multi-point perfect focus system,

567   and an Orca Flash 4.0 CMOS camera. Images were acquired under the following

568   settings: pHluorin (GFP) (488 laser excitation, 525/36 emission), mCherry (561 laser

569   excitation, 630/75 emission), Cy5 (647 nm laser excitation, 705/72 nm emission),

570   Hoechst 33342 Dye (405 nm laser excitation, 455/50 emission) and differential

571   interference contrast (DIC) were used. Acquisition times for each fluorescence channel

572   ranged from 50-600 milliseconds.

573

574   *Single-cell pHi measurements*

575   Prior to imaging, stage top incubator and microscope objectives were pre heated to

576   37°C and kept at 5% CO_2/95% air. Single-cell pHi measurements were performed as

577   previously described[34]. Briefly, initial fields of view (FOV) were collected on the cells in

578   their respective media. Two isotonic buffers (25 mM HEPES, 105 mM KCl, 1 mM $MgCl_2$)

579   were prepared and supplemented with 10 µM nigericin (Thermo Fisher Scientific,

580   N1495). For standardization, isotonic buffers were pre-warmed to 37°C and pH of the

581   "Nigericin buffers" was adjusted to ~6.7 and ~7.7 (with 1M KOH) (recorded for each

582   biological replicate to the hundredths place). For each standardization point, cells were

583   washed three times consecutively with no waiting time with appropriate Nigericin buffer

584   followed by a 5-7 minute equilibration prior to image acquisition. All required buffer

585   exchanges were carried out on the stage incubator to preserve XY positioning. Multiple

586   Z-planes were collected with the center focal plane maintained using the Perfect Focus

587   System (PFS).

588

589   *pHi Image Quantification*

590   NIS Analysis Software was used to quantify pHi. All images were background

591   subtracted using a region of interest (ROI) drawn on glass coverslip (determined by

592   DIC). Individual ROIs were drawn for each cell in each condition (initial, high pH

593   nigericin, and low pH nigericin). For each cell ROI, mean pHluorin and mCherry pixel

594   intensities were quantified and pHluorin/mCherry ratios calculated in Microsoft Excel.

595   For each cell, the nigericin standard fluorescence intensity values were used to

596   generate single-cell standard curves where single-cell pHi was back-calculated based

597   on nigericin buffer pH values reported to the hundredths.

27

598

599

600   *Proliferation Assay*

601   H1299 cells were plated at 1,000 cells/well in a 24 well tissue-culture treated plate on

602   pre-prepared matrix (65 µL/well) (see *Preparation of tunable-stiffness hydrogels*). After

603   24 and 48 hours of culture, cells were lifted via trypsinization (0.25%, Corning, 25-

604   0530Cl) for 20 minutes and counted by hemocytometer.

605

606   *Immunofluorescence Staining*

607   *Fixed Cell Staining*

608   H1299 cells were plated at 75,000 cells/well in 100 µL solution volume on the pre-

609   prepared synthetic ECM plates. After 48 hours, the media was removed and a 3.7%

610   Formaldehyde (Alfa Aesar, 50-000) solution in DPBS was added to each well and

611   allowed to fix at room temperature for 10 minutes. Cells were washed 3x2 minutes with

612   DPBS before a permeabilization solution (0.1% Triton-X (Fisher Scientific, 9002-93-1) in

613   DPBS) was added to each well for ten minutes at room temperature (RT). The Triton-X

614   permeabilization solution was removed and cells were washed 3x2 minutes with DPBS

615   at RT before a blocking solution (1% BSA (Fisher Scientific, BP1600-100) was added to

616   cells for one hour at RT with rocking. The blocking solution was removed and cells were

617   washed 3x2 minutes with DPBS before primary antibody solutions were added to each

618   well and incubated with rocking at 4°C overnight. Primary antibodies were prepared in

619   1% BSA with 0.1% Triton-X at 1:50 dilutions. Primary antibodies used were: β-catenin

620   mouse (BD Biosciences, BDB610154) and FOXC2 rabbit (Cell Signaling Technology,

28

621 12974S). The following day, primary antibody solutions were removed and cells were

622 washed 3x2 minutes with DPBS before secondary antibodies (Goat anti-mouse IgG

623 (H+L) Cross-Absorbed Secondary Antibody, Alexa Fluor 488; Invitrogen; A-11001, Goat

624 anti-rabbit IgG (H+L) Secondary Antibody, Alexa Fluor 488; Invitrogen; A-11008) were

625 added at 1:1,000 in solution of 1% BSA, 0.1% Triton-X, and Hoechst 33342 (DAPI;

626 Thermo Scientific, cat: 62249 were added to each well (1:20,000) in DPBS and

627 incubated with rocking at RT for one hour. Cells were washed 3x2 minutes with DPBS

628 just prior to imaging on the Nikon Ti-2 spinning disk confocal with a 40x oil immersion

629 objective. Images were captured with multiple Z planes to allow visualization of labeled

630 protein colocalization. After acquisition, IMARIS Software (Bitplane, Oxford Instruments,

631 version 9.5.1) and Nikon Elements Analysis software were used to quantify stained

632 proteins. Nuclear pools of proteins were identified using IMARIS software by generating

633 surfaces based on the DAPI channel that represent individual cell nuclei. Mean

634 intensities for all channels within each nuclear surface were exported and analyzed for

635 statistical significance using GraphPad Prism software. Whole cell protein abundance

636 was determined by drawing regions of interest in Nikon Elements Analysis software of

637 single-cells. Mean intensities for all channels were exported and analyzed for statistical

638 significance using GraphPad Prism software.

639

640 *Live Cell Staining*

641 H1299 cells were plated on the pre-prepared synthetic ECM plates 48 hours prior to

642 imaging at 75,000 cells/well in 100 µL solution volume. Images were acquired as

643 outlined in the above sections. Cell nuclei and cell membranes were visualized via

644   Hoechst dye (DAPI; Thermo Scientific, cat: 62249; 1:10,000) and CellMask Deep Red

645   (Thermo Fisher, C10046; 1:20,000), respectively, incubated for 15 minutes at 37º C in

646   complete media. Fields of view were selected by visualizing nuclei (DAPI) and images

647   were collected in the DAPI (30% laser power, 600 ms), GFP (30% laser power, 600

648   ms), Cy5 (30% laser power, 600 ms), and DIC (32.6 DIA, 50 ms) channels. Individual

649   cells were analyzed by IMARIS software by generating cells based on the CellMask

650   channel that represents cell membranes. Cell areas were exported and analyzed for

651   statistical significance using GraphPad Prism software.

652

653   *Single-cell FOXC2 transcriptional activity assay using live-cell microscopy*

654   FOXC2-TAG-Puro expressing H1299 cells were plated on the pre-prepared synthetic

655   ECM plates 48 hours prior to imaging at 75,000 cells/well in 100 µL solution volume.

656   Images were acquired as outlined in the above sections. Cell nuclei and cell

657   membranes were visualized via Hoechst dye (DAPI; Thermo Scientific, cat: 62249;

658   1:10,000) and CellMask Deep Red (Thermo Fisher, C10046; 1:20,000), respectively,

659   incubated for 15 minutes at 37º C in complete media. Fields of view were selected by

660   visualizing nuclei (DAPI) and images were collected in the DAPI (30% laser power, 600

661   ms), GFP (30% laser power, 600 ms), Cy5 (30% laser power, 600 ms), and DIC (32.6

662   DIA, 50 ms) channels. Whole-cell regions of interest (ROIs) were drawn within individual

663   cells using cell mask as a membrane marker and the average GFP intensity for

664   individual cells were exported to Excel. Single-cell intensities were imported to

665   GraphPad Prism for statistical analysis and visualization.

666

667

668

669   *BCECF plate reader assays*

670   Cells were plated at 4.0×10^5–8.0×10^5 cells/well in a 24-well plate and incubated

671   overnight. Cells were treated with 2 µM 2′,7′-bis-(2-carboxyethyl)-5-(and-6)-

672   carboxyfluorescein, acetoxymethyl ester (BCECF-AM; VWR, 89139-244) for 20 min at

673   37°C and 5% CO_2. H1299 parental and NHE1 K.O. cells were washed three times for 5

674   min each time with a pre-warmed (37°C) HEPES-based wash buffer (30 mM HEPES pH

675   7.4, 145 mM NaCl, 5 mM KCl, 10 mM glucose, 1 mM $MgSO_4$, 1 mM $KHPO_4$, 2 mM

676   $CaCl_2$, pH 7.4) to match their low bicarbonate medium (RPMI) and NHE1 K.O. Bicarb.

677   cells were washed three times for 5 min each time with a pre-warmed (37°C) HEPES-

678   based wash buffer (30 mM HEPES pH 7.4, 95 mM NaCl, 5 mM KCl, 10 mM glucose, 1

679   mM $MgSO_4$, 1 mM $KHPO_4$, 2 mM $CaCl_2$, pH 7.4) to match sodium bicarbonate

680   treatment. For standardization, three calibration buffers (25 mM HEPES, 105 mM KCl, 1

681   mM $MgCl_2$) were supplemented with 10 µM nigericin (Thermo Fisher Scientific, N1495),

682   pH was adjusted to ~6.7, ~7.0, and ~7.7, and were pre-warmed to 37°C. Fluorescence

683   was read (excitation of 440 and 490 nm, both with emission at 535 nm) on a Cytation 5

684   (BioTek) plate reader incubated at 37°C with 5% CO_2. Kinetic reads were taken at 15-s

685   intervals for 5 min, using a protocol established within BioTek Gen5 software. After the

686   initial pHi read, the HEPES/bicarbonate wash was aspirated and replaced with one of

687   the nigericin buffer standards, and cells were incubated at 37°C with 5% CO_2 for 7 min.

688   BCECF fluorescence was read by the plate reader as above. This process was

689   repeated with the second nigericin standard. As it takes significant time to equilibrate

31

690   CO_2 in the plate reader, we did not measure nigericin standardizations without CO_2. The

691   mean intensity ratio (490/440 values) was derived from each read. Measurements were

692   calculated from a nigericin linear regression using exact nigericin buffer pH to two

693   decimal places (Grillo-Hill et al., 2014).

694

695   *NHE1 Recovery Assay*

696   40,000 cells were plated in the first two rows of a 24-well plate two days prior to

697   transfection (one row of H1299 parental, the other H1299 NHE1 K.O.). Cells were

698   loaded with 10uM SNARF in serum free media and incubated in the dark at 37° C for

699   30min. Each well was washed three times at 37°C for 5 minutes with a HEPES buffer

700   (30mM HEPES pH-7.4, 115mM NaCl, 5mM KCl, 10mM glucose, 1mM $MgSO_4$, 1mM

701    $KHPO_4$, 2mM $CaCl_2$). The cells were imaged using a BioTek Cytation5 in imager mode.

702   The SNARF was imaged with SNARF cube (531x/586m) and TexasRed cube

703   (586x/647m). Images were taken approximately every two minutes which was the

704   shortest interval allowed by the imager mode software for two rows of a 24-well plate.

705   Initial baseline images were taken in the HEPES buffer at pH 7.4 at 3 time points

706   (approx. 6 mins total). Next, cells were loaded with ammonium chloride using a HEPES-

707   based ammonium chloride buffer (30mM HEPES pH-7.4, 30mM NH_4Cl, 115mM NaCl,

708   5mM KCl, 10mM glucose, 1mM $MgSO_4$, 1mM $KHPO_4$, 2mM $CaCl_2$) and cells were

709   imaged for 3 time points (approx. 6min). An acid load was induced by removing the

710   ammonium chloride buffer and replacing it with the HEPES buffer (no NH_4Cl) with or

711   without NHE1 inhibitor (10 μM EIPA (5-(*N*-ethyl-*N*-isopropyl) amiloride), Chemscene,

712   CS-7935). Cells were imaged while they recovered (7 time points, approx. 14 minutes).

713   A calibration curve was then obtained by imaging the cells in nigericin containing buffers

714   at the various pH's, around 7.5 (6 time points, approx. 12min), 7.0 (4 time points,

715   approx. 8min), and 6.5 (4 time points, approx. 8min). The standard curve was then used

716   to back calculate the pHi of the cells during the experiment. The data was normalized to

717   the initial point of the recovery period to look at the recovery rate.

718

719   *Statistical analysis*

720   GraphPad Prism was used to prepare graphs and perform statistical analyses. All data

721   sets were subject to normality tests (D'Angostino & Pearson, Anderson-Darling,

722   Shapiro-Wilk, and Kolmogorov-Smirnov) and outlier analyses using the ROUT method

723   (Q=1%). For non-normally distributed data, a Kruskal–Wallis test with Dunn's multiple

724   comparisons correction was used (Figures 1-5) For fold increase in cell number and

725   population pHi data, one-way ANOVA was used (Figure 2E, 5D). All significance was

726   indicated in figures by the following: *$P<0.05$; **$P<0.01$; ***$P<0.001$; ****$P<0.0001$.

727

728   **Online Supplementary Materials:** Online supplementary materials include Figure S1-

729   S6.

730

736

737 **Author contributions:** Conceptualization: LML, KAW, DH-P; Methodology: LML, KAW,

738 LA, KJT DH-P; Validation: LML, KAW, DH-P; Formal analysis:, LML, LA, LNM, EH, JH,

739 KJT, KAW, DH-P; Investigation: LML, LA, LNM, EH, JH; Resources: KAW, DH-P.; Data

740 collection: LML, LA, LNM, EH, JH, KJT; Data curation: LML, LA, LNM, EH, JH, KJT,

741 KAW, DH-P; Writing – original draft: LML, KAW; Writing - review & editing: LML, LA,

742 LNM, EH, JH, KJT, DH-P; Visualization: LML, LNM, KAW, DH-P; Supervision: KAW,

743 DH-P; Project administration: KAW, DH-P; Funding acquisition: LML, KAW, DH-P.

744

745 **Competing Interests:** Authors declare no competing interests.

746

753

754 **References**

755 (1) Walker, C.; Mojares, E.; del Río Hernández, A. Role of Extracellular Matrix in Development
756 and Cancer Progression. *Int. J. Mol. Sci.* **2018**, *19* (10), 3028.
757 https://doi.org/10.3390/ijms19103028.
758 (2) Carey, S. P.; Martin, K. E.; Reinhart-King, C. A. Three-Dimensional Collagen Matrix
759 Induces a Mechanosensitive Invasive Epithelial Phenotype. *Sci. Rep.* **2017**, *7* (1), 42088.
760 https://doi.org/10.1038/srep42088.

761 (3) Wechman, S. L.; Emdad, L.; Sarkar, D.; Das, S. K.; Fisher, P. B. Vascular Mimicry:
762   Triggers, Molecular Interactions and in Vivo Models. *Adv. Cancer Res.* **2020**, *148*, 27–67.
763   https://doi.org/10.1016/bs.acr.2020.06.001.
764 (4) Webb, B. A.; Chimenti, M.; Jacobson, M. P.; Barber, D. L. Dysregulated pH: A Perfect
765   Storm for Cancer Progression. *Nat. Rev. Cancer* **2011**, *11* (9), 671–677.
766   https://doi.org/10.1038/nrc3110.
767 (5) White, K. A.; Grillo-Hill, B. K.; Barber, D. L. Cancer Cell Behaviors Mediated by
768   Dysregulated pH Dynamics at a Glance. *J. Cell Sci.* **2017**, *130* (4), 663–669.
769   https://doi.org/10.1242/jcs.195297.
770 (6) Reshkin, S. J.; Greco, M. R.; Cardone, R. A. Role of pHi, and Proton Transporters in
771   Oncogene-Driven Neoplastic Transformation. *Philos. Trans. R. Soc. B Biol. Sci.* **2014**, *369*
772   (1638), 20130100. https://doi.org/10.1098/rstb.2013.0100.
773 (7) Gilkes, D. M.; Semenza, G. L.; Wirtz, D. Hypoxia and the Extracellular Matrix: Drivers of
774   Tumour Metastasis. *Nat. Rev. Cancer* **2014**, *14* (6), 430–439.
775   https://doi.org/10.1038/nrc3726.
776 (8) Bordeleau, F.; Mason, B. N.; Lollis, E. M.; Mazzola, M.; Zanotelli, M. R.; Somasegar, S.;
777   Califano, J. P.; Montague, C.; LaValley, D. J.; Huynh, J.; Mencia-Trinchant, N.; Negrón
778   Abril, Y. L.; Hassane, D. C.; Bonassar, L. J.; Butcher, J. T.; Weiss, R. S.; Reinhart-King, C.
779   A. Matrix Stiffening Promotes a Tumor Vasculature Phenotype. *Proc. Natl. Acad. Sci. U. S.*
780   *A.* **2017**, *114* (3), 492–497. https://doi.org/10.1073/pnas.1613855114.
781 (9) DuChez, B. J.; Doyle, A. D.; Dimitriadis, E. K.; Yamada, K. M. Durotaxis by Human Cancer
782   Cells. *Biophys. J.* **2019**, *116* (4), 670–683. https://doi.org/10.1016/j.bpj.2019.01.009.
783 (10)   Nallanthighal, S.; Heiserman, J. P.; Cheon, D.-J. The Role of the Extracellular Matrix in
784   Cancer Stemness. *Front. Cell Dev. Biol.* **2019**, *7*, 86.
785   https://doi.org/10.3389/fcell.2019.00086.
786 (11)   Bevensee, M. O.; Boron, W. F. EFFECTS OF ACUTE HYPOXIA ON
787   INTRACELLULAR-pH REGULATION IN ASTROCYTES CULTURED FROM RAT
788   HIPPOCAMPUS. *Brain Res.* **2008**, *1193*, 143–152.
789   https://doi.org/10.1016/j.brainres.2007.12.002.
790 (12)   Burbridge, M. F.; West, D. C.; Atassi, G.; Tucker, G. C. The Effect of Extracellular pH
791   on Angiogenesis in Vitro. *Angiogenesis* **1999**, *3* (3), 281–288.
792   https://doi.org/10.1023/a:1009092511894.
793 (13)   Ulmschneider, B.; Grillo-Hill, B. K.; Benitez, M.; Azimova, D. R.; Barber, D. L.; Nystul,
794   T. G. Increased Intracellular pH Is Necessary for Adult Epithelial and Embryonic Stem Cell
795   Differentiation. *J. Cell Biol.* **2016**, *215* (3), 345–355. https://doi.org/10.1083/jcb.201606042.
796 (14)   Liu, Y.; White, K. A.; Barber, D. L. Intracellular pH Regulates Cancer and Stem Cell
797   Behaviors: A Protein Dynamics Perspective. *Front. Oncol.* **2020**, *10*, 1401.
798   https://doi.org/10.3389/fonc.2020.01401.
799 (15)   Choi, C.-H.; Webb, B. A.; Chimenti, M. S.; Jacobson, M. P.; Barber, D. L. pH Sensing
800   by FAK-His58 Regulates Focal Adhesion Remodeling. *J. Cell Biol.* **2013**, *202* (6), 849–859.
801   https://doi.org/10.1083/jcb.201302131.
802 (16)   Czowski, B. J.; Romero-Moreno, R.; Trull, K. J.; White, K. A. Cancer and pH Dynamics:
803   Transcriptional Regulation, Proteostasis, and the Need for New Molecular Tools. *Cancers*
804   **2020**, *12* (10), 2760. https://doi.org/10.3390/cancers12102760.

805 (17)   Czowski, B. J.; White, K. A. Intracellular pH Regulates β-Catenin with Low pHi
806   Increasing Adhesion and Signaling Functions. March 27, 2024.
807   https://doi.org/10.1101/2024.03.22.586349.
808 (18)   Benton, G.; Arnaoutova, I.; George, J.; Kleinman, H. K.; Koblinski, J. Matrigel: From
809   Discovery and ECM Mimicry to Assays and Models for Cancer Research. *Adv. Drug Deliv.*
810   *Rev.* **2014**, *79–80*, 3–18. https://doi.org/10.1016/j.addr.2014.06.005.
811 (19)   Kim, P. K.; Halbrook, C. J.; Kerk, S. A.; Radyk, M.; Wisner, S.; Kremer, D. M.;
812   Sajjakulnukit, P.; Andren, A.; Hou, S. W.; Trivedi, A.; Thurston, G.; Anand, A.; Yan, L.;
813   Salamanca-Cardona, L.; Welling, S. D.; Zhang, L.; Pratt, M. R.; Keshari, K. R.; Ying, H.;
814   Lyssiotis, C. A. Hyaluronic Acid Fuels Pancreatic Cancer Cell Growth. *eLife 10*, e62645.
815   https://doi.org/10.7554/eLife.62645.
816 (20)   Deng, B.; Zhao, Z.; Kong, W.; Han, C.; Shen, X.; Zhou, C. Biological Role of Matrix
817   Stiffness in Tumor Growth and Treatment. *J. Transl. Med.* **2022**, *20* (1), 540.
818   https://doi.org/10.1186/s12967-022-03768-y.
819 (21)   Fan, F.; Su, B.; Kolodychak, A.; Ekwueme, E.; Alderfer, L.; Saha, S.; Webber, M. J.;
820   Hanjaya-Putra, D. Hyaluronic Acid Hydrogels with Phototunable Supramolecular Cross-
821   Linking for Spatially Controlled Lymphatic Tube Formation. *ACS Appl. Mater. Interfaces*
822   **2023**, *15* (50), 58181–58195. https://doi.org/10.1021/acsami.3c12514.
823 (22)   Hanjaya-Putra, D.; Yee, J.; Ceci, D.; Truitt, R.; Yee, D.; Gerecht, S. Vascular Endothelial
824   Growth Factor and Substrate Mechanics Regulate in Vitro Tubulogenesis of Endothelial
825   Progenitor Cells. *J. Cell. Mol. Med.* **2010**, *14* (10), 2436–2447.
826   https://doi.org/10.1111/j.1582-4934.2009.00981.x.
827 (23)   Albeiroti, S.; Soroosh, A.; de la Motte, C. A. Hyaluronan's Role in Fibrosis: A
828   Pathogenic Factor or a Passive Player? *BioMed Res. Int.* **2015**, *2015*, e790203.
829   https://doi.org/10.1155/2015/790203.
830 (24)   Nemec, S.; Ganda, S.; Al Taief, K.; Kopecky, C.; Kuchel, R.; Lebhar, H.; Marquis, C. P.;
831   Thordarson, P.; Kilian, K. A. A Tunable Tumor Microenvironment through Recombinant
832   Bacterial Collagen-Hyaluronic Acid Hydrogels. *ACS Appl. Bio Mater.* **2022**.
833   https://doi.org/10.1021/acsabm.2c00186.
834 (25)   Alderfer, L.; Russo, E.; Archilla, A.; Coe, B.; Hanjaya-Putra, D. Matrix Stiffness Primes
835   Lymphatic Tube Formation Directed by Vascular Endothelial Growth Factor-C. *FASEB J.*
836   *Off. Publ. Fed. Am. Soc. Exp. Biol.* **2021**, *35* (5), e21498.
837   https://doi.org/10.1096/fj.202002426RR.
838 (26)   Piersma, B.; Hayward, M.-K.; Weaver, V. M. Fibrosis and Cancer: A Strained
839   Relationship. *Biochim. Biophys. Acta Rev. Cancer* **2020**, *1873* (2), 188356.
840   https://doi.org/10.1016/j.bbcan.2020.188356.
841 (27)   Cooper, J.; Giancotti, F. G. Integrin Signaling in Cancer: Mechanotransduction,
842   Stemness, Epithelial Plasticity, and Therapeutic Resistance. *Cancer Cell* **2019**, *35* (3), 347–
843   367. https://doi.org/10.1016/j.ccell.2019.01.007.
844 (28)   Gan, Z.; Qin, X.; Liu, H.; Liu, J.; Qin, J. Recent Advances in Defined Hydrogels in
845   Organoid Research. *Bioact. Mater.* **2023**, *28*, 386–401.
846   https://doi.org/10.1016/j.bioactmat.2023.06.004.
847 (29)   Pickup, M. W.; Mouw, J. K.; Weaver, V. M. The Extracellular Matrix Modulates the
848   Hallmarks of Cancer. *EMBO Rep.* **2014**, *15* (12), 1243–1253.
849   https://doi.org/10.15252/embr.201439246.

850   (30)   Vanderhooft, J. L.; Alcoutlabi, M.; Magda, J. J.; Prestwich, G. D. Rheological Properties
851   of Cross-Linked Hyaluronan-Gelatin Hydrogels for Tissue Engineering. *Macromol. Biosci.*
852   **2009**, *9* (1), 20–28. https://doi.org/10.1002/mabi.200800141.
853   (31)   Mammoto, A.; Connor, K. M.; Mammoto, T.; Yung, C. W.; Huh, D.; Aderman, C. M.;
854   Mostoslavsky, G.; Smith, L. E. H.; Ingber, D. E. A Mechanosensitive Transcriptional
855   Mechanism That Controls Angiogenesis. *Nature* **2009**, *457* (7233), 1103–1108.
856   https://doi.org/10.1038/nature07765.
857   (32)   Slater, K.; Partridge, J.; Nandivada, H.; Usa, M. Tuning the Elastic Moduli of Corning®
858   Matrigel® and Collagen I 3D Matrices by Varying the Protein Concentration.
859   (33)   Soofi, S. S.; Last, J. A.; Liliensiek, S. J.; Nealey, P. F.; Murphy, C. J. The Elastic
860   Modulus of Matrigel^{TM} as Determined by Atomic Force Microscopy. *J. Struct. Biol.* **2009**,
861   *167* (3), 216–219. https://doi.org/10.1016/j.jsb.2009.05.005.
862   (34)   Spear, J. S.; White, K. A. Single-Cell Intracellular pH Dynamics Regulate the Cell Cycle
863   by Timing the G1 Exit and G2 Transition. *J. Cell Sci.* **2023**, *136* (10), jcs260458.
864   https://doi.org/10.1242/jcs.260458.
865   (35)   Koivusalo, M.; Welch, C.; Hayashi, H.; Scott, C. C.; Kim, M.; Alexander, T.; Touret, N.;
866   Hahn, K. M.; Grinstein, S. Amiloride Inhibits Macropinocytosis by Lowering
867   Submembranous pH and Preventing Rac1 and Cdc42 Signaling. *J. Cell Biol.* **2010**, *188* (4),
868   547–563. https://doi.org/10.1083/jcb.200908086.
869   (36)   Grillo-Hill, B. K.; Webb, B. A.; Barber, D. L. Ratiometric Imaging of pH Probes.
870   *Methods Cell Biol.* **2014**, *123*, 429–448. https://doi.org/10.1016/B978-0-12-420138-5.00023-
871   9.
872   (37)   Liu, Y.; Reyes, E.; Castillo-Azofeifa, D.; Klein, O. D.; Nystul, T.; Barber, D. L.
873   Intracellular pH Dynamics Regulates Intestinal Stem Cell Lineage Specification. *Nat.*
874   *Commun.* **2023**, *14* (1), 3745. https://doi.org/10.1038/s41467-023-39312-9.
875   (38)   Martin, C.; Pedersen, S. F.; Schwab, A.; Stock, C. Intracellular pH Gradients in
876   Migrating Cells. *Am. J. Physiol.-Cell Physiol.* **2011**, *300* (3), C490–C495.
877   https://doi.org/10.1152/ajpcell.00280.2010.
878   (39)   Williamson, S. C.; Metcalf, R. L.; Trapani, F.; Mohan, S.; Antonello, J.; Abbott, B.;
879   Leong, H. S.; Chester, C. P. E.; Simms, N.; Polanski, R.; Nonaka, D.; Priest, L.; Fusi, A.;
880   Carlsson, F.; Carlsson, A.; Hendrix, M. J. C.; Seftor, R. E. B.; Seftor, E. A.; Rothwell, D. G.;
881   Hughes, A.; Hicks, J.; Miller, C.; Kuhn, P.; Brady, G.; Simpson, K. L.; Blackhall, F. H.;
882   Dive, C. Vasculogenic Mimicry in Small Cell Lung Cancer. *Nat. Commun.* **2016**, *7*, 13322.
883   https://doi.org/10.1038/ncomms13322.
884   (40)   Racordon, D.; Valdivia, A.; Mingo, G.; Erices, R.; Aravena, R.; Santoro, F.; Bravo, M.
885   L.; Ramirez, C.; Gonzalez, P.; Sandoval, A.; González, A.; Retamal, C.; Kogan, M. J.; Kato,
886   S.; Cuello, M. A.; Osorio, G.; Nualart, F.; Alvares, P.; Gago-Arias, A.; Fabri, D.; Espinoza,
887   I.; Sanchez, B.; Corvalán, A. H.; Pinto, M. P.; Owen, G. I. Structural and Functional
888   Identification of Vasculogenic Mimicry in Vitro. *Sci. Rep.* **2017**, *7* (1), 6985.
889   https://doi.org/10.1038/s41598-017-07622-w.
890   (41)   Schnellmann, R.; Ntekoumes, D.; Choudhury, M. I.; Sun, S.; Wei, Z.; Gerecht, S.
891   Stiffening Matrix Induces Age-Mediated Microvascular Phenotype Through Increased Cell
892   Contractility and Destabilization of Adherens Junctions. *Adv. Sci.* **2022**, *9* (22), 2201483.
893   https://doi.org/10.1002/advs.202201483.
894   (42)   Delgado-Bellido, D.; Zamudio-Martínez, E.; Fernández-Cortés, M.; Herrera-Campos, A.
895   B.; Olmedo-Pelayo, J.; Perez, C. J.; Expósito, J.; de Álava, E.; Amaral, A. T.; Valle, F. O.;

Diaz, A. G.; Oliver, F. J. VE-Cadherin Modulates β-Catenin/TCF-4 to Enhance Vasculogenic Mimicry. *Cell Death Dis.* **2023**, *14* (2), 135. https://doi.org/10.1038/s41419-023-05666-7.

(43) Qi, L.; Song, W.; Liu, Z.; Zhao, X.; Cao, W.; Sun, B. Wnt3a Promotes the Vasculogenic Mimicry Formation of Colon Cancer via Wnt/β-Catenin Signaling. *Int. J. Mol. Sci.* **2015**, *16* (8), 18564–18579. https://doi.org/10.3390/ijms160818564.

(44) Xu, X.; Zhang, Y.; Wang, X.; Li, S.; Tang, L. Substrate Stiffness Drives Epithelial to Mesenchymal Transition and Proliferation through the NEAT1-Wnt/β-Catenin Pathway in Liver Cancer. *Int. J. Mol. Sci.* **2021**, *22* (21), 12066. https://doi.org/10.3390/ijms222112066.

(45) Astudillo, P. Extracellular Matrix Stiffness and Wnt/β-Catenin Signaling in Physiology and Disease. *Biochem. Soc. Trans.* **2020**, *48* (3), 1187–1198. https://doi.org/10.1042/BST20200026.

(46) Sun, M.; Chi, G.; Xu, J.; Tan, Y.; Xu, J.; Lv, S.; Xu, Z.; Xia, Y.; Li, L.; Li, Y. Extracellular Matrix Stiffness Controls Osteogenic Differentiation of Mesenchymal Stem Cells Mediated by Integrin A5. *Stem Cell Res. Ther.* **2018**, *9* (1), 52. https://doi.org/10.1186/s13287-018-0798-0.

(47) White, K. A.; Grillo-Hill, B. K.; Esquivel, M.; Peralta, J.; Bui, V. N.; Chire, I.; Barber, D. L. β-Catenin Is a pH Sensor with Decreased Stability at Higher Intracellular pH. *J. Cell Biol.* **2018**, *217* (11), 3965–3976. https://doi.org/10.1083/jcb.201712041.

(48) Cannell, I. G.; Sawicka, K.; Pearsall, I.; Wild, S. A.; Deighton, L.; Pearsall, S. M.; Lerda, G.; Joud, F.; Khan, S.; Bruna, A.; Simpson, K. L.; Mulvey, C. M.; Nugent, F.; Qosaj, F.; Bressan, D.; Dive, C.; Caldas, C.; Hannon, G. J. FOXC2 Promotes Vasculogenic Mimicry and Resistance to Anti-Angiogenic Therapy. *Cell Rep.* **2023**, *42* (8). https://doi.org/10.1016/j.celrep.2023.112791.

(49) Cha, B.; Geng, X.; Mahamud, M. R.; Fu, J.; Mukherjee, A.; Kim, Y.; Jho, E.-H.; Kim, T. H.; Kahn, M. L.; Xia, L.; Dixon, J. B.; Chen, H.; Srinivasan, R. S. Mechanotransduction Activates Canonical Wnt/β-Catenin Signaling to Promote Lymphatic Vascular Patterning and the Development of Lymphatic and Lymphovenous Valves. *Genes Dev.* **2016**, *30* (12), 1454–1469. https://doi.org/10.1101/gad.282400.116.

(50) Koch, S. Regulation of Wnt Signaling by FOX Transcription Factors in Cancer. *Cancers* **2021**, *13* (14), 3446. https://doi.org/10.3390/cancers13143446.

(51) Gozo, M. C.; Aspuria, P.-J.; Cheon, D.-J.; Walts, A. E.; Berel, D.; Miura, N.; Karlan, B. Y.; Orsulic, S. Foxc2 Induces Wnt4 and Bmp4 Expression during Muscle Regeneration and Osteogenesis. *Cell Death Differ.* **2013**, *20* (8), 1031–1042. https://doi.org/10.1038/cdd.2013.34.

(52) Grillo-Hill, B. K.; Choi, C.; Jimenez-Vidal, M.; Barber, D. L. Increased H+ Efflux Is Sufficient to Induce Dysplasia and Necessary for Viability with Oncogene Expression. *eLife* **2015**, *4*, e03270. https://doi.org/10.7554/eLife.03270.

(53) Amith, S. R.; Wilkinson, J. M.; Fliegel, L. Assessing Na+/H+ Exchange and Cell Effector Functionality in Metastatic Breast Cancer. *Biochim. Open* **2016**, *2*, 16–23. https://doi.org/10.1016/j.biopen.2016.01.001.

(54) Hulikova, A.; Harris, A. L.; Vaughan-Jones, R. D.; Swietach, P. Regulation of Intracellular pH in Cancer Cell Lines under Normoxia and Hypoxia. *J. Cell. Physiol.* **2013**, *228* (4), 743–752. https://doi.org/10.1002/jcp.24221.

(55) Konen, J.; Summerbell, E.; Dwivedi, B.; Galior, K.; Hou, Y.; Rusnak, L.; Chen, A.; Saltz, J.; Zhou, W.; Boise, L. H.; Vertino, P.; Cooper, L.; Salaita, K.; Kowalski, J.; Marcus,

942   A. I. Image-Guided Genomics of Phenotypically Heterogeneous Populations Reveals
943   Vascular Signalling during Symbiotic Collective Cancer Invasion. *Nat. Commun.* **2017**, *8*,
944   15078. https://doi.org/10.1038/ncomms15078.
945   (56)   Andersen, A. P.; Flinck, M.; Oernbo, E. K.; Pedersen, N. B.; Viuff, B. M.; Pedersen, S. F.
946   Roles of Acid-Extruding Ion Transporters in Regulation of Breast Cancer Cell Growth in a
947   3-Dimensional Microenvironment. *Mol. Cancer* **2016**, *15* (1), 45.
948   https://doi.org/10.1186/s12943-016-0528-0.
949